Macromolecular Journals

Macromolecular Chemistry and Physics

Effect of Organoclay on the Orientation and Thermal Properties of Liquid-Crystalline Polymers

Jayita Bandyopadhyay, Suprakas Sinha Ray,* Mosto Bousmina*

The preparation and thermal and thermo-mechanical properties of nanocomposites based on liquid-crystalline polymers (LCP) and organically-modified layered silicate (OMLS) is described. From XRD patterns, very little smectic ordering is present in the pure LCP; in the nanocomposites, the polymer chains tended to orient in the direction of the dispersed clay layers. According to the DSC results, during first heating, the first melting peak represents the crystalline to nematic transition and, after that, a broader isotropization takes place. Although TGA of the samples showed a single-step decomposition through chain scission under an inert atmosphere, in air the nanocomposites underwent a two-step process, with onset of degradation at a higher temperature. The first step is mainly due to chain scission and the second is due to oxidative reactions.

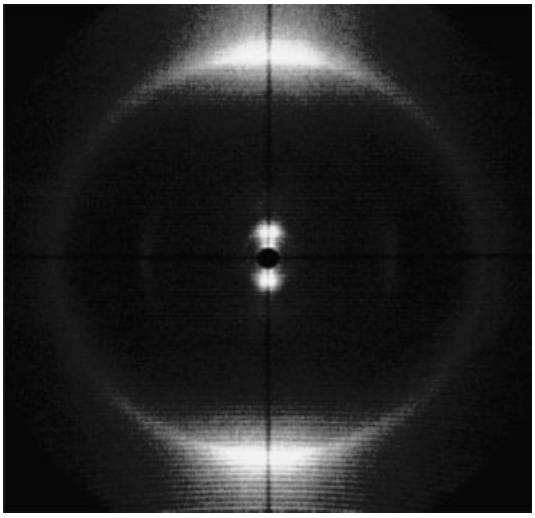

Introduction

Liquid-crystalline polymers (LCP) are well known for their excellent properties, such as high strength and stiffness, low melt viscosity, and their high chemical and thermal resistance.[1,2] Recently, the blending of thermotropic LCP with thermoplastics has attracted much attention because of the self-reinforcement effect of LCP due to their rigid-rod-like molecular structure. In such LCP/thermoplastics blends, the LCP acts as reinforcing element like nanoclay in nanocomposites by offering a large surface area. The advantages of incorporation of a few percent of LCP in thermoplastic matrices are: (i) improvement in processability because of the lower viscosity of the LCP, and (ii) the improvement in mechanical properties by uniform microfibrillation of the LCP in the matrix polymer.[3] Over the last decade, many polymers such as poly(propylene),[4] polystyrene,[5] poly(methyl methacrylate),[6] poly(ethylene terephthalate),[7] poly(vinyl alcohol),[8] poly(butylene succinate),[9] and polylactide,[9b,10] have been used for the preparation of nanocomposites with either pure or organically-modified clay. However, there remain very few reports regarding LCP-based nanocomposites with clay. Vaia et al.[11] reported the reversible intercalation between organoclay and LCP in the nematic state. According to them, much better intercalation of polymer chains in the clay galleries is possible with a prolonged annealing time. Zhang et al.[12] showed that

J. Bandyopadhyay, M. Bousmina
Department of Chemical Engineering, Laval University, Quebec, Canada G1K 7P4
E-mail: bousmina@gch.ulvala.ca
S. Sinha Ray
National Centre for Nano-Structured Materials, Council for Scientific and Industrial Research, PO Box 395, Pretoria 0001, Republic of South Africa
Fax: +27 12 841 2135; E-mail: rsuprakas@csir.co.za

DOI: 10.1002/macp.200700350

the glass-transition temperature and the mechanical properties of LCP/clay nanocomposites were enhanced compared to virgin polymer. Recently, Huang et al.[13] reported on the dispersion characteristics and rheology of nanocomposites based on organoclay and thermotropic LCP with pendent functional groups. In another report[14] they confirmed the very high degree of dispersion of organoclay in the LCP matrix, because of the formation of hydrogen bonds between the pendent pyridyl group in the LCP and the hydroxyl group of the surfactant residing at the surface of organoclay. According to Shen et al.[15] the polar epoxy groups in liquid-crystalline epoxides make it possible to diffuse into the clay galleries. The modifier present in the organoclay catalyzes the epoxy ring-opening reaction with a diamine curing agent. Chang et al.[16] also prepared aromatic thermotropic LCP nanocomposites and focused on the morphology and thermal properties. Up to now, however, nobody has focused on how the structure of the LCP changes after the preparation of the nanocomposites with organoclay, and how the clay particles affect the properties of the LCP. Therefore, the main objective of this study is to understand the effect of the organoclay on the structure of the LCP and hence on the mesophase transitions and crystallization, and on the thermo-mechanical properties of the LCP. Thermogravimetric analyses (TGA) have been carried out to determine the inorganic part present in the nanocomposite samples and the thermal stability of the nanocomposite samples under both oxidative and inert environments.

Experimental Part

Materials

The commercially-available, main-chain, thermotropic liquid-crystalline polymer, Vectra B950, used to prepare the LCP-organoclay nanocomposites was supplied by Ticona. The chemical formula of Vectra B950 is shown in Figure 1.

The organoclay Closite® 20A (C20A) was purchased from Southern Clay Products. It is a natural montmorillonite (MMT) modified by dimethyl dihydrogenated-tallow quaternary ammonium salt with cation exchange capacity of 95 meq per 100 g.[17] Figure 2 shows the molecular formula of the surfactant.

The polar solubility parameters (δ) for the LCP and organic modifier of C20A were estimated roughly from the group-contribution method of Fedors[18] and the values were 25.6 $J^{1/2}\cdot cm^{-3/2}$ and 16.9 $J^{1/2}\cdot cm^{-3/2}$ respectively. The reason for selecting C20A for the preparation of the nanocomposites was the higher thermal stability of the surfactant of C20A compared to other Closite clays at the processing temperature, and the larger interlayer spacing between the silicate layers (2.45 nm, estimated from the XRD results). To determine the thermal stability of C20A at the processing conditions, the TGA ramp test was performed and, according to this result, C20A lost ≈8% of its initial weight at 270 °C in 25 min. The C20A sample was kept at 270 °C for 5 min and it showed an extra ≈4% weight loss. Since the nanocomposites were prepared by melt extrusion where the residence time of the samples inside the extruder was ≤2 min, the degradation of C20A didn't significantly affect the properties of the nanocomposites. All of these materials were dried at 110 °C for 24 h under vacuum before blending to avoid degradation caused by moisture. The thermal treatment also improves the performance of the LCP, such as a dramatic improvement in tenacity. This improvement is usually due to the increase in molecular weight, as well as in the degree of perfection of the crystallinity.[1]

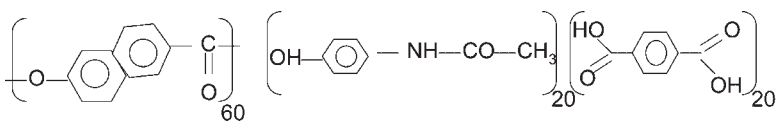

Figure 1. Molecular structure of Vectra B950.

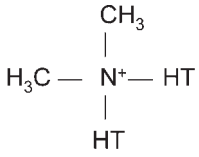

(HT: ~65% C18, ~30% C16, ~5% C14)

Figure 2. Molecular structure of the surfactant used for the modification of MMT.

Nanocomposite Preparation

Nanocomposites were prepared by melt extrusion in a Haake twin-screw extruder at a screw speed of 30 rpm. The barrel temperatures used were 260, 270, and 270 °C and the temperature of the capillary die was 270 °C. After collecting the nanocomposite samples from the extruder, they were dried under vacuum at 110 °C for 24 h to remove any water and then moulded under different conditions, according to the needs of different experiments. Initially the samples were moulded using a Carver laboratory press at 300 °C, under 2 MPa pressure for 2 min, and the sample thicknesses were ≈1.2 mm. For the study of non-isothermal crystallization kinetics, the sheet of highly-crystalline samples was prepared by using a Carver model: 4393.4PR3B02 at 300 °C, under 2 kg pressure for 2 min, and then slowly cooled for about 4 h by passing air through the plates.

Characterization Techniques and Conditions

All of the characterizations were carried out using isothermally-annealed, moulded samples. The X-ray- diffraction analyses in the small-angle ($2\theta = 0–30^\circ$) and wide-angle ($2\theta = 21–69^\circ$) regions were performed using a Simens-500 diffractometer in the transmission mode. The beam was Cu K_α ($\lambda = 0.154$ nm) operated at 40 kV, and 40 mA.

The morphology of the fractured surface of the moulded nanocomposites was investigated by scanning electron microscopy (SEM, JEOL model JSM-820 apparatus) operated at an accelerating voltage of 15 kV. The samples were fractured in

Macromol. Chem. Phys. **2007**, *208*, 1979–1991

Macromolecular Journals

DOI: 10.1002/macp.200700350

liquid nitrogen and then sputter-coated with gold/palladium (50/50), to enhance the conductivity.

The dispersability of the clay platelets in the LCP matrix was determined by means of TEM, (JEOL model JEM 1230 instrument). The samples were epoxy-mounted and ultramicrotomed with a diamond knife. The sample thicknesses were kept within a range of 50–70 nm.

In order to detect the phase transitions, differential scanning calorimetry (DSC model: TA Q100) was used. For conventional DSC, the temperature and the energy readings were calibrated against indium. The thermal transitions of all three samples (as-received LCP and as-prepared nanocomposites) were studied by conventional DSC. In order to do that, all of the samples went through the same experimental cycle: heating from room temperature to 350 °C at a rate of 10 °C · min^{-1}, then cooling to 20 °C at the same rate as heating and further heating up to 350 °C at a heating rate of 10 °C · min^{-1}. To study the non-isothermal crystallization dynamics, the samples were melted at 350 °C at a heating rate of 20 °C · min^{-1}, kept at that temperature for 5 min to destroy all the previous thermal history, cooled to 20 °C at different cooling rates: 5, 10, 20 and 30 °C · min^{-1} and then re-melted up to 350 °C at a heating rate of 20 °C · min^{-1} as soon as cooling was finished. The DSC samples were weighed such that all of the samples had an identical LCP content. The sample weight was maintained at low levels (3–4 mg) for all measurements in order to minimize any possible thermal lag during the scans.

The thermo-mechanical properties of the LCP and its nanocomposites were examined using a Rheometric Scientific Analyzer (RSA) in dual-cantilever bending mode. The storage flexural modulus (E'), loss modulus (E'') and tanδ values were determined at a constant frequency of 6.283 rad · s^{-1}, with a strain amplitude of 0.02% (determined after the strain sweep tests at different temperatures), a heating rate of 2 °C·min^{-1} and in the temperature range 0 to 200 °C.

Thermo-Gravimetric Analyses (TGA) were carried out by using a TA Q500 instrument in the temperature range 25 to 900 °C under both air and nitrogen atmospheres. The amount of the inorganic part present in the nanocomposite samples was determined using TGA. According to TGA data (conducted under air), the amount of the inorganic part present in the first batch nanocomposite sample was 1.4% and that in the second batch nanocomposite sample was 3.4%; hence the abbreviations used for these nanocomposites were LCPCN1.4 and LCPCN3.4, respectively.

Results and Discussion

Structure of the Nanocomposites

The XRD patterns not only provide information about the dispersion of the silicate layers in the polymer matrix,[19] but also the mesophase structures present in the LCP and the orientation of the directors can be predicted from the X-ray diffractograms.[20] The most well-known technique, XRD in the small-angle region, was used to determine the intercalation of polymer chains in the nanoclay galleries. Figure 3 shows the XRD patterns of the pure C20A powder and nanocomposites in the small-angle region. The characteristic (001) peak of the C20A powder appeared at $2\theta = 3.6°$ ($d = 2.45$ nm). In both nanocomposites the characteristic peak intensity of C20A was not only significantly reduced due to the dilution effect of clay but also shifted to $2\theta = 2.28°$ and $2\theta = 2.32°$ for LCPCN1.4 and LCPCN3.4, respectively. These peak shifts towards lower angles indicate the intercalation of polymer chains inside the clay galleries. The variation of clay content, however, doesn't show a significant change in the basal spacing: in both nanocomposites it remains almost the same ($d = 3.85$ nm). Thus it is expected that the dispersion of the clay platelets in the polymer matrix should be better in the LCPCN1.4 nanocomposite sample. The XRD patterns plotted in the range $2\theta = 8$ to 27° are shown in Figure 4. It is clear from the Figure that the nanocomposites have the same mesophase structure or, in other words, the same type of crystal formation at $2\theta \approx 11.8°$ and $2\theta \approx 19.4°$. In the case of nanocomposites, however, a shoulder peak accompanied with the second crystalline peak appears. This may be due to the growth of the same kind of crystal with a different size distribution or orientation. The XRD analyses in the wide-angle region show the formation of different types of crystals in the nanocomposite samples as compared to neat LCP (Figure 5). The effect of clay concentration on the crystal growth can be visualised directly in the XRD pattern at $2\theta \approx 43.2°$. The XRD powder patterns in Figure 6 and 7, show the diffraction patterns of the oriented samples[21] and also show how the orientation of the LCP crystallites changed after addition of organically-modified layered silicate (OMLS) in various proportions. Thus it is possible to tune the orientation of LCP by adding the filler. For extruded materials, the structure and mechanical properties were found to be closely related to the extrusion conditions.[2,3] Thus the

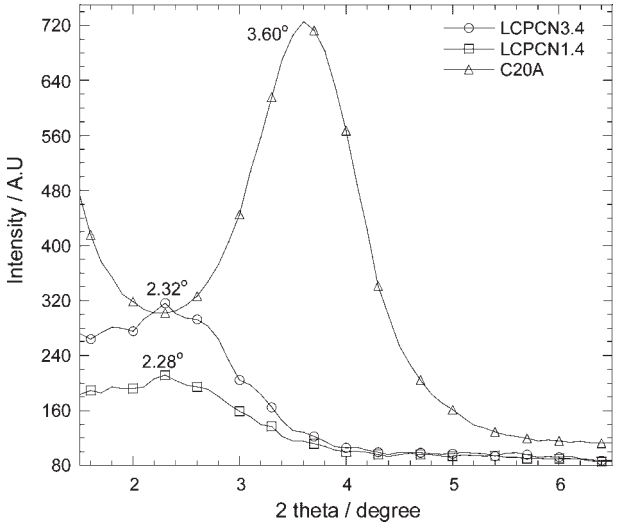

Figure 3. X-ray diffraction patterns of organoclay powder and LCP nanocomposites with two different wt.-% of organoclay loading.

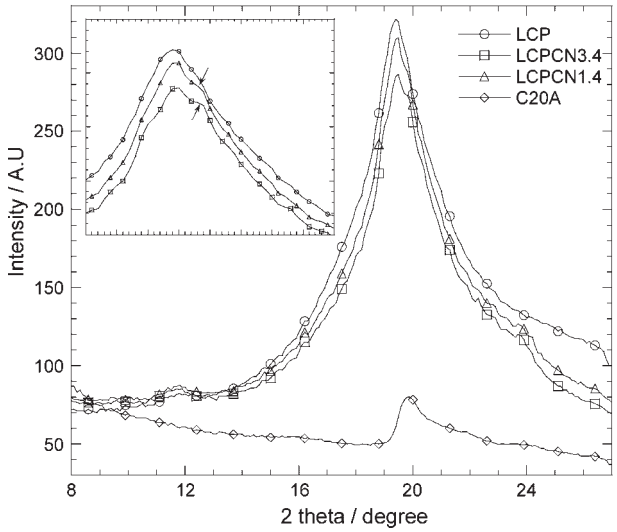

Figure 4. X-ray diffraction patterns of organoclay and LCP nanocomposites with two different wt.-% of organoclay loading in the crystalline region.

orientation of LCP in nanocomposites may depend on factors such as the draw ratio of the extruder, and the condition of moulding for example. Here, the effect of these above-mentioned factors were minimized by moulding all the samples under the same conditions. Although C20A hasn't too much interaction with the Vectra B950, it can change the mesophase structure. It is clear from Figure 6 that because of the ordered structure of the layered silicate, nanocomposites exhibit more and more ordered structures, compared to the pure polymer, with an increase in nanoclay loading. From Figure 6 it is prominent that LCP exhibits diffuse rings with a sharp ring as an outer shell, whereas the nanocomposites exhibit sharp and

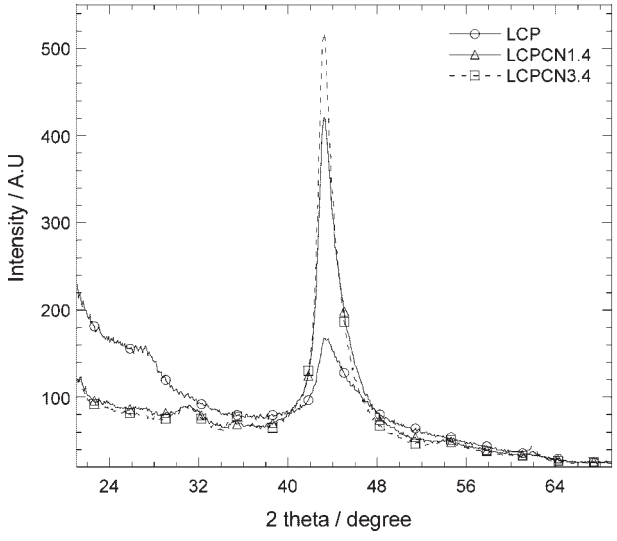

Figure 5. Wide-angle X-ray diffraction (WAXD) patterns of the nanocomposites with two different wt.-% of organoclay loading.

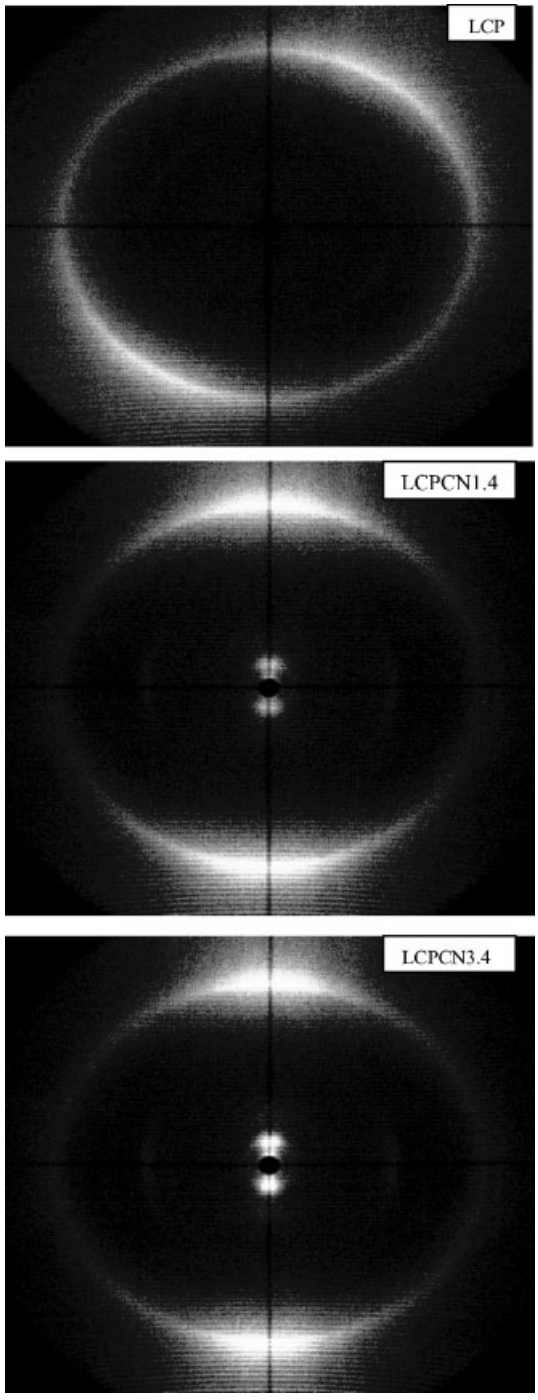

Figure 6. XRD powder patterns in the small-angle region.

intense diffractions at the shell and in the core. The nematic phase is characterized by the molecules having no positional order, rather than they tend to align in the same direction. On the other hand, in the smectic phase the molecules maintain the general orientational order of the nematic phase, but also tend to align themselves in layers.

Macromol. Chem. Phys. **2007**, *208*, 1979–1991

Macromolecular Journals

DOI: 10.1002/macp.200700350

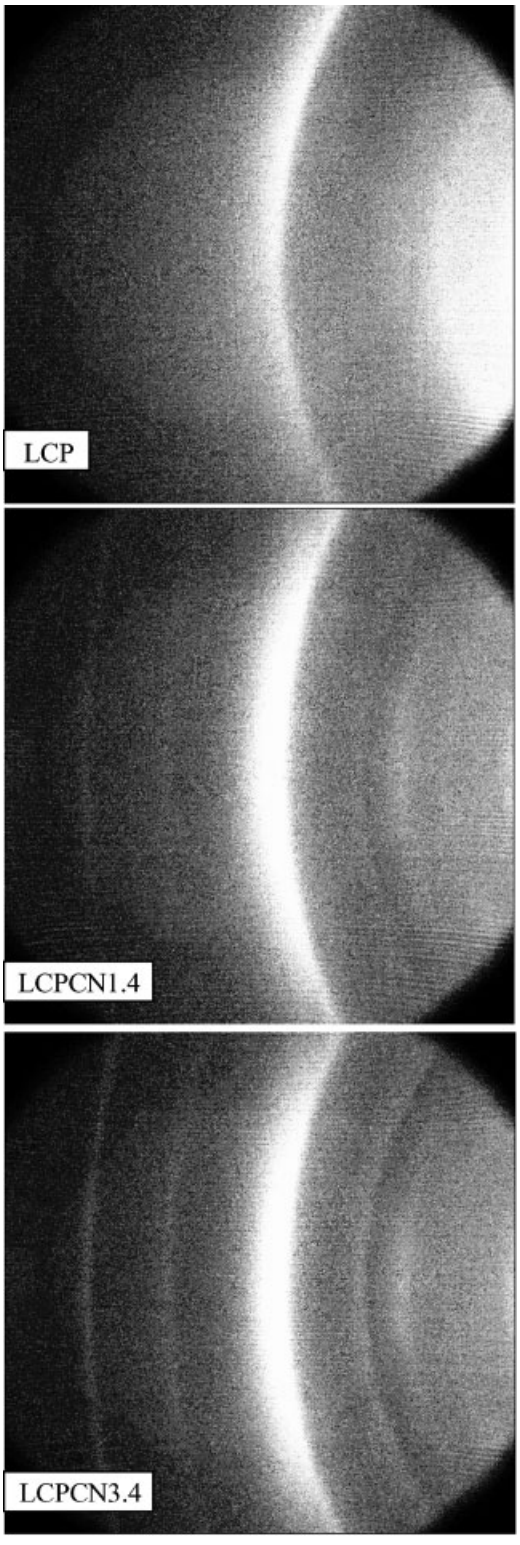

Figure 7. XRD powder patterns in the wide-angle region.

Although detailed studies on the mesophase transition and crystal growth are ongoing, one can expect from Figure 6 and 7 that very little smectic-like ordering is present in the pure LCP, whereas in the nanocomposites, polymer chains not only tend to orient in the direction of the dispersed clay layers, but the ordering in alignment is also improved.

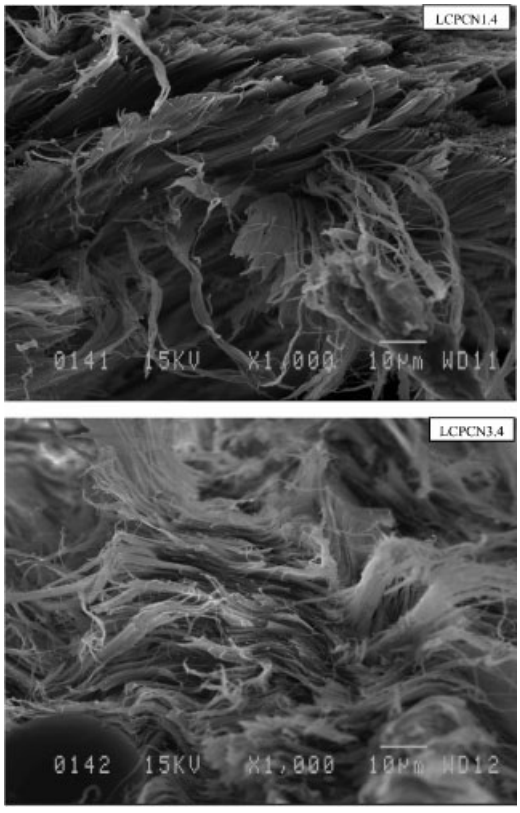

Figure 8. SEM images of the LCPCN1.4 and LCPCN3.4 nanocomposites.

SEM images of the LCP/clay nanocomposites are shown in Figure 8. The only thing observed here is that the fracture surfaces of these nanocomposites have a febrile morphology. The dispersion of the clay platelets in the LCP matrix can be visualized by the TEM observations shown in Figure 9. The intercalated clay layers can be visualized directly as the black entities in the TEM images.[22] The TEM images show that the dispersion of organoclay is much better with a lower clay concentration and an increase in the clay concentration results in more and more agglomeration and hence almost no change in the basal spacing.

Thermal Properties

Melting and Crystallization Behavior of Virgin Polymer and As-Prepared Nanocomposite Samples

To study the mesophase transitions and crystal-growth behavior of all of the samples, the method mentioned in

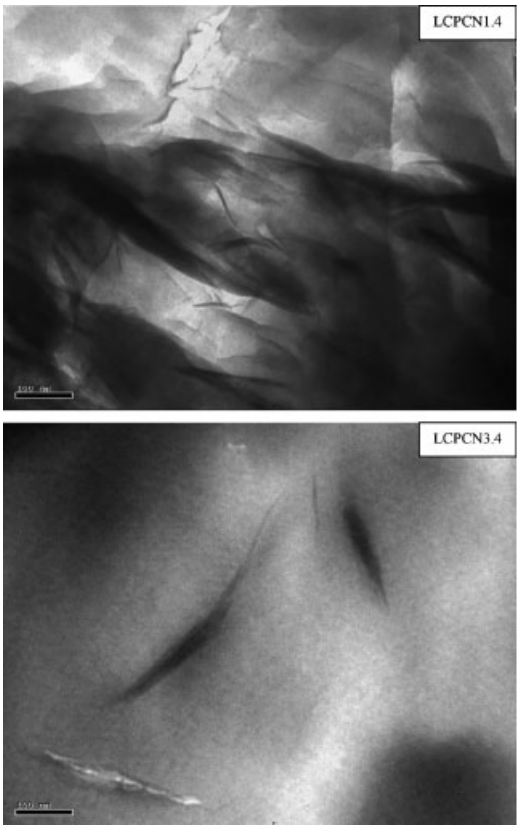

Figure 9. TEM images of the LCPCN1.4 and LCPCN3.4 nanocomposites.

the characterization part was followed. Different parts of Figure 10 represent respectively (a) the first heating, (b) cooling and (c) subsequent heating. Different thermal parameters determined from the cooling and the second heating cycles are tabulated in Table 1. According to Figure 10a the T_g of neat LCP was affected after addition of organically-modified layered silicate. In the nanocomposites, chain relaxation associated with the T_g is possibly due to the enhancement of ordering in the direction of the clay lamellae. A further increase in temperature resulted in a sharp transition that is associated with a wider one. The first melting peak represents the crystalline to nematic transition and after that a broader isotropization takes place.

During cooling from the isotropic state, as shown in Figure 10b and Table 1, the crystallization-onset temperature ($T_{c,on}$) shifted towards higher temperatures. This is due to the nucleation effect of the organoclay, by offering a large surface area to start the crystallization. The crystallization-peak temperatures (T_c) however remained almost the same, for the samples examined here. The enthalpy of crystallization (ΔH_c) also remained almost unaltered after addition of the clay. It is noticeable that LCP and its nanocomposites showed a very small value of the transition enthalpy because their chain rigidity prevents molecules folding, and the mesophase transitions generally occur by segregation of the rigid chain molecules.[1] The half time of crystallization ($t_{½}$), defined as the time required to attain a relative degree of crystallinity of 50%, can be estimated from the Equation (1).

$$t_{1/2} = \frac{T_{c,on} - T_c}{\phi} \quad (1)$$

where, ϕ is the cooling rate. The results are summarized in Table 1. It is clear from Table 1 that the $t_{½}$ value of the nanocomposite samples remains almost the same as that of the pure polymer.

During the second heating, as observed in Figure 10c, the enthalpy-relaxation phenomena associated with T_g is not as prominent as in first heating cycle. According to Table 1, the T_g of pure polymer remained unaltered in the nanocomposite samples with lower clay content, but it shifted towards slightly lower temperatures when the clay loading increased. This indicates that with increase an in the clay concentration, the movement of chain segments starts earlier. As soon as the samples cross ≈200 °C, a complex but continuous phase transition or consecutive melting - recrystallization/crystal orientation - remelting mechanism takes place. A comprehensive study of the phase morphology is still under investigation.

The temperatures of the two prominent and one broad transition were denoted by T_{m1}, T_{m2} and T_{m3}, respectively in Table 1. Chung et al.[1] have already reported that, depending on the annealing time, during isothermal crystallization Vectra B950 shows sometimes two or sometimes one melting peak. Here, according to Figure 10d, it is clear that, the pure Vectra B950 exhibited very little crystal orientation just before T_{m2}; the nanocomposites exhibited a more pronounced crystal-orientation effect at 270.75 °C and 269 °C for LCPCN1.4 and LCPCN3.4 respectively. Since Vectra B950 is a fully-aromatic, main-chain random copolymer, the distribution of molecular sequences within the polymer itself may not be so even. Further, in contrast to ref.,[1] chain rigidity prevents molecules folding, and the transitions generally occur by segregation of rigid-chain molecules. Probably, because of these reasons LCP shows such a complex melting phenomenon and incorporation of the organoclay creates further complexity. The appearance of three endothermic peaks in the DSC also supports the XRD results. From the XRD patterns (Figure 6 and 7) it was clear that the smectic-like ordering improved in the nanocomposites and also with an increase in clay loading. Thus the three melting peaks in the DSC thermogram originates from (i) melting, T_{m1}; (ii) transition from a more-ordered structure (smectic) to a less ordered structure (nematic), T_{m2}; and (iii)

Macromolecular Journals
DOI: 10.1002/macp.200700350

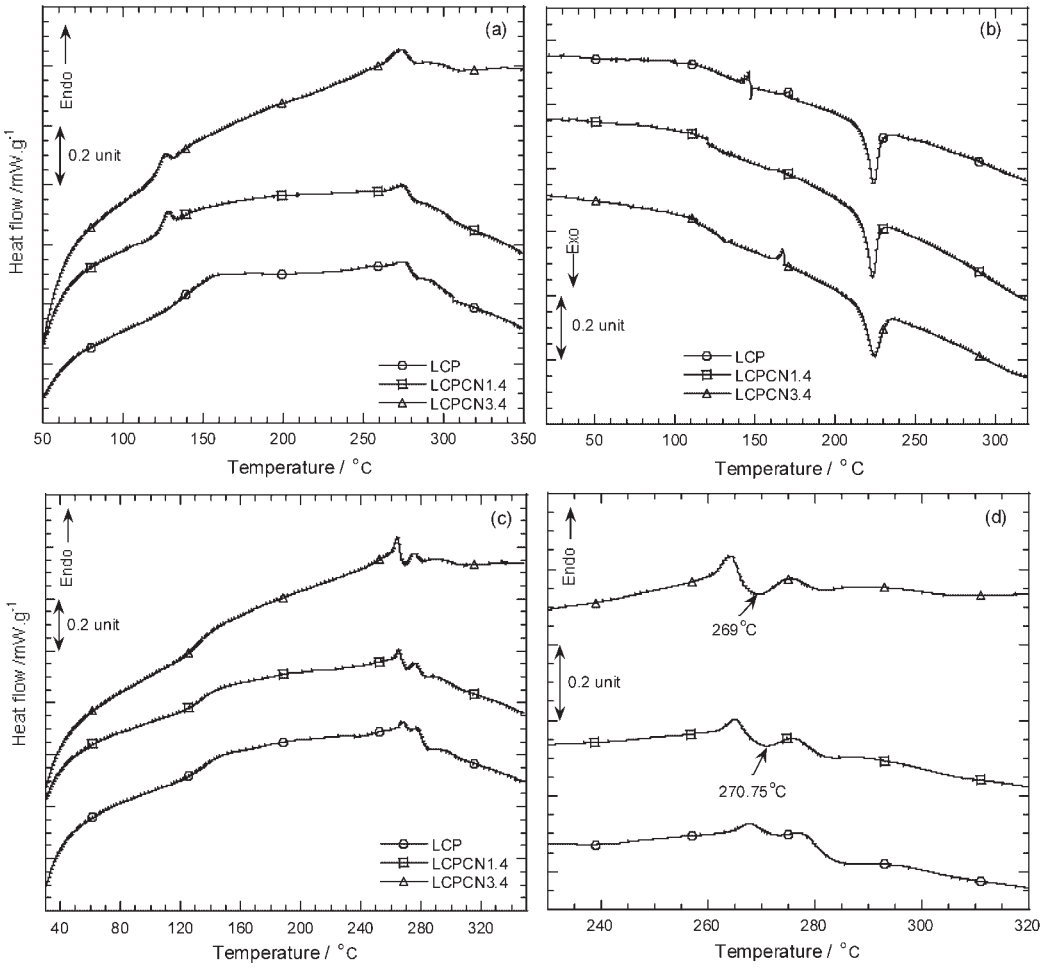

Figure 10. DSC thermograms of the as-received LCP sample and as-prepared nanocomposites during (a) first heating, (b) consecutive cooling, (c) second heating and (d) enlarged view of second heating cycle.

isotropization, T_{m3}. According to Table 1, for the nanocomposite samples T_{m1}, T_{m2} and T_{m3} were shifted towards the lower-temperature region, compared to the virgin VectraB950 sample, because organoclay facilitates the segregation of the rigid chains of Vectra B950. Since organoclay induces a more and more ordered structure in the nanocomposites, the values of the enthalpy of fusion (ΔH_f) increase with the clay loading as reported in Table 1.

Non-Isothermal Crystallization Behavior

The characteristic parameters of non-isothermal crystallization (from the cooling and second heating runs) are tabulated in Table 2. Figure 11 and 12 represent, respectively, the exothermic and endothermic plots during non-isothermal crystallization and subsequent heating. According to Table 2 for all the three samples studied here, the crystallization-peak temperature (T_c) shifted towards

Table 1. DSC results for as-received and as-prepared samples (from cooling and second heating run).

Sample	$T_{c,\,on}$	T_c	ΔH_c	$t_{1/2}$	T_g	T_{m1}	T_{m2}	T_{m3}	ΔH_f
	°C	°C	J · g^{-1}	min	°C	°C	°C	°C	J · g^{-1}
LCP	232.22	223.90	2.39	0.83	134.01	267.77	277.11	293.99	5.47
LCPCN1.4	236.83	223.11	3.15	1.37	134.21	265.22	276.16	291.09	7.15
LCPCN3.4	238.28	224.42	3.31	1.39	132.13	264.22	275.33	290.67	8.06

lower temperature with an increase in the cooling rate because, with an increased cooling rate, the molten samples experience a shorter time to crystallize and hence complete crystallization was not possible with higher rates. For nanocomposite samples, however, there is no significant change in the T_c and ΔH_c values.

The effect of the cooling rate and clay concentration on the subsequent heating scan can be visualized directly in Figure 12. For LCP, at a lower cooling rate (5 °C · min^{-1}) the two transition processes are clearly visible. With an increase in the cooling rate (10 °C · min^{-1}), the first transition (T_{m1}) shifted slightly towards a higher temperature and the second transition (T_{m2}) shifted toward a lower temperature. A further increase in the cooling rate resulted in the two transitions being merged into one, with a further reduction of the ΔH_f values. The LCPCN1.4 nanocomposite sample also exhibited a similar trend to the pure LCP sample. The increase in clay content resulted in the presence of two distinguishable transitions for a cooling rate of 20 °C · min^{-1}. With an increase in the clay content, the intensity of the first transition was enhanced. In all three samples, however, (especially noticeable in LCPCN3.4 sample) the intensity of the first transition reduced and the second one improved, and finally at a heating rate 30 °C · min^{-1}, the two transitions merged into one. These observations can be explained as follows: with a decreased cooling rate during non-isothermal crystallization, the samples get more time to organize crystals and as a result there is a possibility of attaining a more-ordered structure. Thus, during heating the first thermal event corresponds to a more-ordered to less-ordered transition and the second thermal event corresponds to isotropization.

Dynamic Mechanical Analysis (DMA)

Dynamic mechanical analyses were carried out to understand the response of the pure LCP and its nanocomposites to an oscillatory deformation under the bending mode as a function of temperature. The effect of organo-filler on the storage flexural modulus (E'), loss modulus (E'') and tanδ values were respectively recorded in Figure 13a, b, and c. The improvement of both moduli of the nanocomposites and, of course, with an increase in the filler concentration in the whole range of temperature studied here, is because of the reinforcement effect of the organoclay.[19] Although the first relaxation process is not so prominent in Figure 13a, a relaxation at around 40 °C affects the viscous behavior and hence the glass-rubber transition. The DSC thermogram (Figure 10c) also supports this relaxation phenomenon. The tanδ (the ratio E'/E'') generally determines the molecular-mobility transitions, such as T_g. According to Figure 13c, the nanocomposites also show the same relaxation process like LCP, but the first relaxation (first tanδ peak) shifts towards lower temperatures for the nanocomposite samples, compared to virgin polymer. The second tanδ peak (which is comparable to the T_g values reported in Table 1) remained unaltered after addition of the clay. The temperatures corresponding to these tanδ peaks are given in Table 3.

Thermogravimetric Analysis

The thermogravimetric analyses were carried out under both nitrogen and air atmosphere. Figure 14 and 15 show the thermogravimetric analysis (TGA) and derivative thermogravimetric analysis (DTGA) curves under the nitrogen and air atmosphere respectively. Under an inert

Table 2. The characteristic parameters of non-isothermal crystallization (from cooling and second heating run).

Sample	ϕ	T_c	ΔH_c	T_{m1}	T_{m2}	ΔH_f
	°C · min^{-1}	°C	J · g^{-1}	°C	°C	J · g^{-1}
LCP	5	226.81	2.35	265.04	275.83	4.10
	10	223.35	2.42	265.73	274.17	3.21
	20	219.55	2.59	266.89	–	2.29
	30	218.14	2.61	273.64	–	2.21
LCPCN1.4	5	226.02	3.12	262.84	273.96	3.32
	10	222.60	3.12	262.72	272.95	2.85
	20	219.37	2.64	263.04	–	1.19
	30	217.63	2.68	273.22	–	0.97
LCPCN3.4	5	225.44	2.82	259.81	271.06	4.18
	10	221.53	2.57	261.15	272.27	3.94
	20	217.63	2.08	260.76	272	2.58
	30	216.39	2.28	259.60	–	2.78

Macromolecular Journals
DOI: 10.1002/macp.200700350

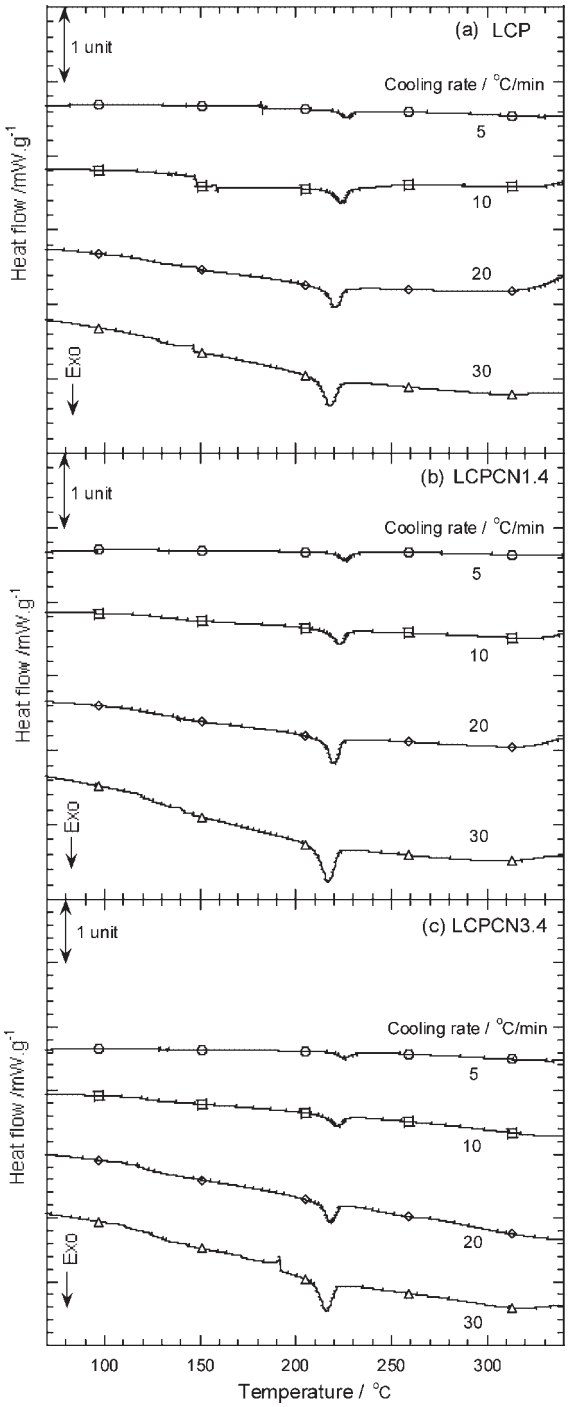

Figure 11. DSC thermograms of non-isothermal crystallization (exotherms) for (a) LCP, (b) LCPCN1.4 and (c) LCPCN3.4 nanocomposites.

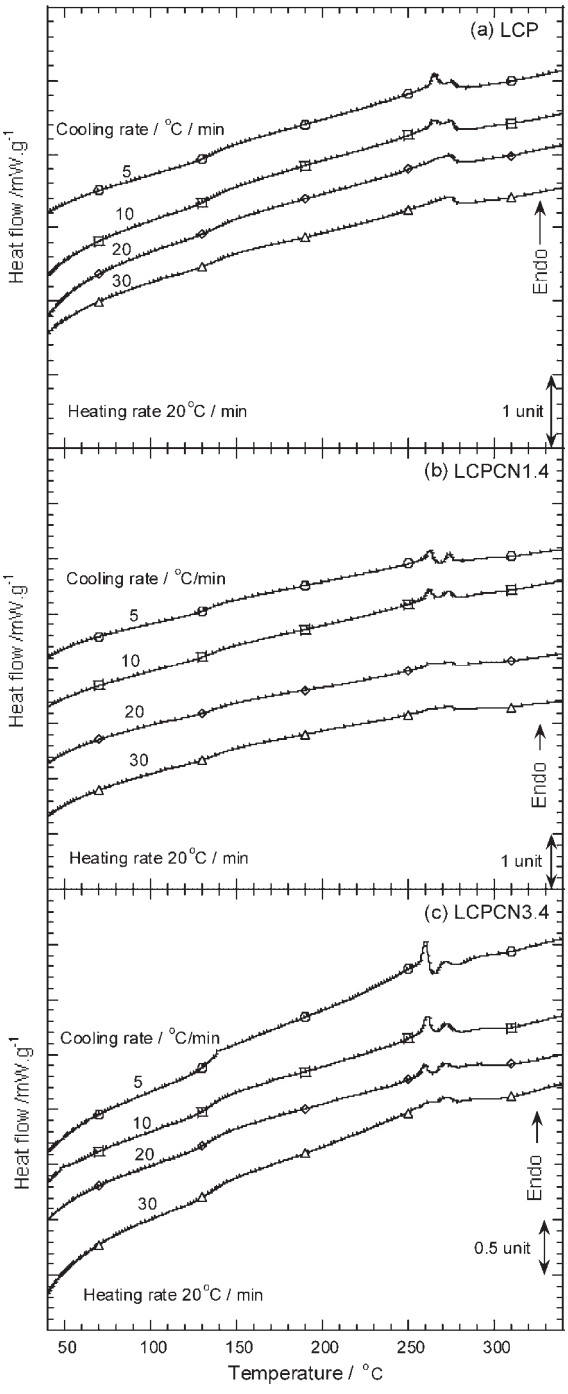

Figure 12. DSC thermograms of non-isothermal crystallization (endotherms) for (a) LCP, (b) LCPCN1.4, and (c) LCPCN3.4 nanocomposites.

atmosphere, the polymer shows a single-step decomposition by random chain scission of the polymer,[1] as determined by both the TGA and the DTGA curve in Figure 14. In the case of the nanocomposite samples, initially the degradation starts a little earlier because of the decomposition of the organic modifier present in the organoclay,[23] but after around 8% degradation the nanocomposites show a much higher thermal stability. If 10% of degradation is considered to be the onset of the main degradation process, then, according to Table 4, the nanocomposites exhibit a higher stability against thermal decomposition, compared to pure LCP. Thus, at this stage,

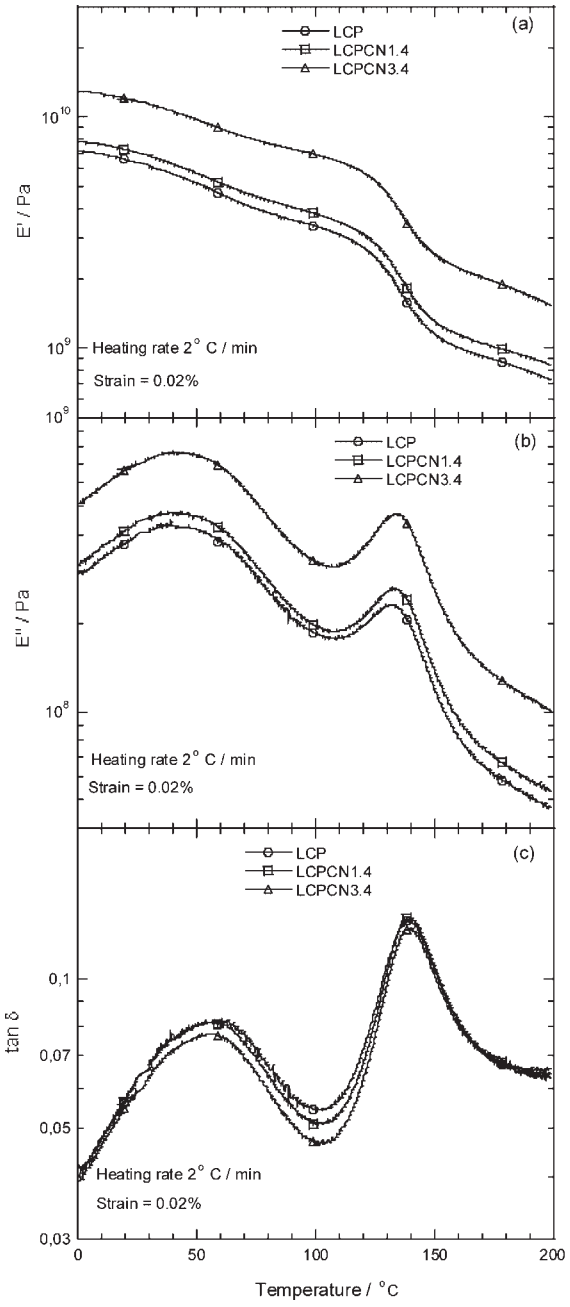

Figure 13. DMA data for LCP and its nanocomposites: (a) storage flexural modulus, (b) loss modulus and (c) tanδ as a function of temperature.

the clay platelets act as an insulator; in the course of the heating, however, they act as a heat source and enhance char formation at a lower temperature.[24] For better dispersion of the nanoclay in the LCPCN1.4 sample, the char formation starts faster than in the other nanocomposites. The DTGA curves of the nanocomposites show a very small, but distinct, transition at 448 °C and 432 °C for the LCPCN1.4 and LCPCN3.4 samples respectively. The probable reason is that the dispersion of clay platelets in

Table 3. The characteristic parameters determined from the dynamic mechanical analyses.

Sample	$T_{tan\delta 1}$	$T_{tan\delta 2}$
	°C	°C
LCP	61.67	138.89
LCPCN1.4	57.22	138.89
LCPCN3.4	56.11	138.89

the LCP matrix results in some chain scission of the long, rigid LCP chains and these small-length chains decompose by further chain scission at a lower temperature. Finally

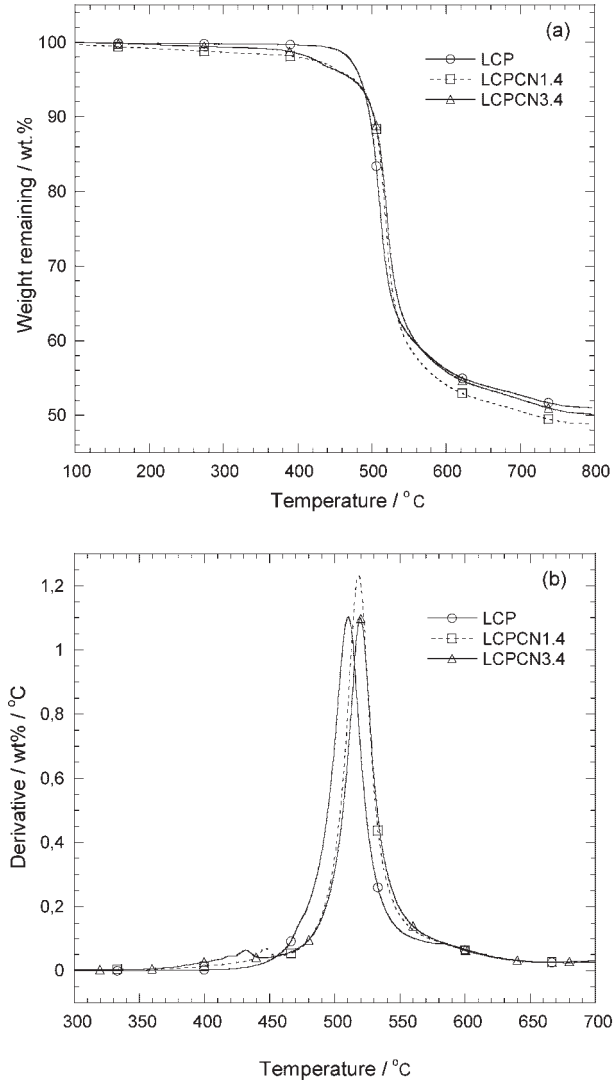

Figure 14. a) TGA thermograms and b) first-derivative TGA (DTGA) curves of neat LCP and its nanocomposites under nitrogen atmosphere.

DOI: 10.1002/macp.200700350

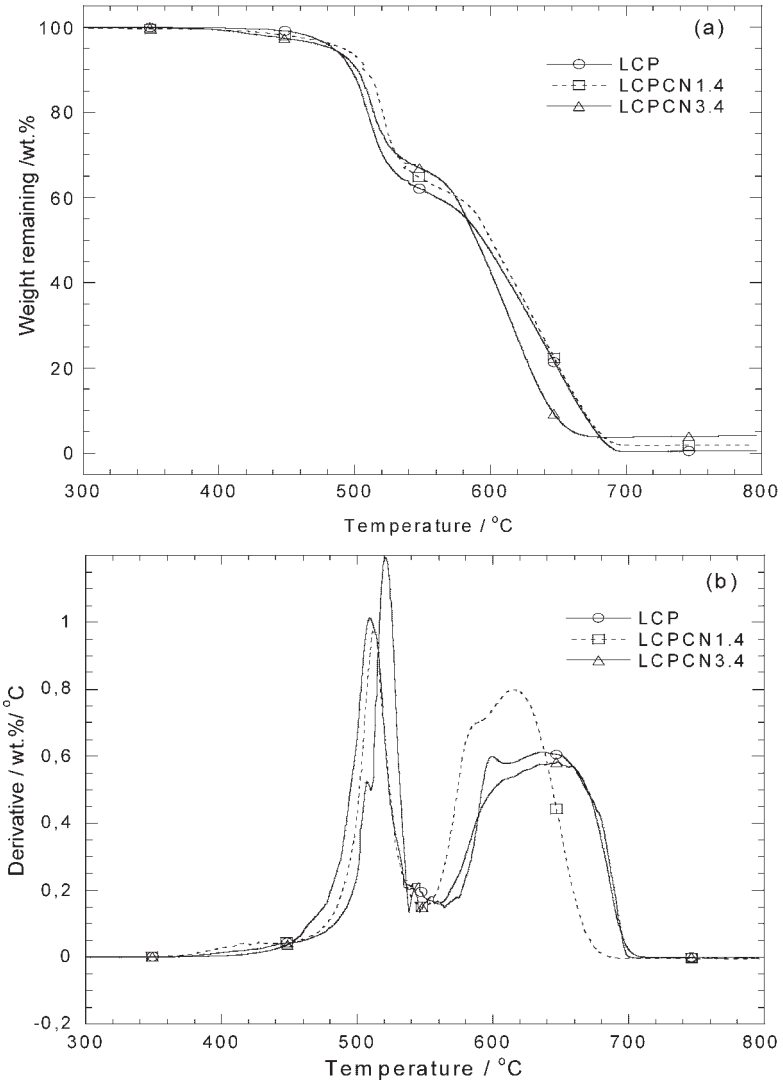

Figure 15. a) TGA thermograms and b) first derivative TGA (DTGA) curves of neat LCP and its nanocomposites under air atmosphere.

the maximum decomposition also occurs by structure-bond rupture or by chain scission.

Like under an inert atmosphere, in an air atmosphere, the nanocomposites exhibit higher values of the onset of degradation, as reported in Table 4. According to Chung et al.[1] Vectra B950 shows two-step decompositions under air atmosphere: the first degradation step is mainly due to chain scission, with some extent of oxidation, and the second degradation step is due to oxidative reactions. Thus the first step is mainly a charring process and the second step is a char-combustion process. In the DTGA curves in Figure 15b, the first intense peak represents the char formation process and the second intense peak represents the char combustion process. Here also, the nanocomposites exhibit a two-step char formation process, like under the inert atmosphere, and a two-step char-combustion process.

Table 4. Onset degradation temperature of neat LCP and its nanocomposites determined from TGA.

Sample	Onset degradation (≈10% weight loss) temperature	
	under nitrogen	under air
	°C	°C
LCP	496.7	497.5
LCPCN1.4	502.5	507.5
LCPCN3.4	502.5	502.5

Conclusion

In order to study the effect of organically-modified layered silicate on the structure, orientation and hence the other properties of LCP, nanocomposites of LCP were prepared with two different amounts of layered-silicate loading. XRD diffraction patterns in the small-angle region were used to determine the intercalation of the polymer chains in the nanoclay galleries. In both nanocomposites the characteristic peak intensity of C20A was not only significantly reduced due to the dilution effect of clay, but also shifted towards the lower-angle side, indicating the intercalation of polymer chains inside the clay galleries. The effect of clay concentration on the crystal growth can be visualized directly in the XRD patterns in the wide-angle region. The XRD patterns in both the small- and wide-angle regions represent the diffraction patterns of the oriented samples and also show how the orientation of the crystallites changed after addition of organoclay with different concentrations. Thus it is possible to tune the orientation of LCP by adding the filler. From these patterns one can expect that very little smectic-like ordering is present in the pure LCP, whereas in the nanocomposites, the molecules not only tend to orient in the direction of dispersed clay layers, but the ordering in alignment also improved.

SEM images of the fracture surfaces of the LCP/clay nanocomposites show a febrile morphology. TEM images show the dispersion of organoclay is much better with a lower clay concentration and that an increase in clay concentration results in more and more agglomeration.

During the first heating cycle of as-prepared samples, analyzed by DSC, the T_g of the neat LCP was affected after

addition of organically-modified layered silicate. In the nanocomposites, the chain relaxation associated with the T_g is possibly due to an enhancement of the ordering in the direction of the clay lamellae. A further increase in temperature results in a sharp transition associated with a wider one. The first melting peak represents the crystalline to nematic transition, and after that, a broader isotropization takes place. The crystallization-peak temperatures (T_c) of the LCP remained the same after nanocomposite preparation. During subsequent heating after crystallization, the T_g of the pure polymer remained unchanged in the nanocomposites with the lower clay content, but shifted toward a slightly lower temperature region when the clay percentage increased. This indicates that, with an increase in clay loading, the movement of the chain segments starts earlier. Consistent with the XRD patterns, the appearance of the three melting peaks in the DSC thermogram can be concluded as (i) melting, T_{m1}; (ii) transition from a more-ordered structure (smectic) to a less-ordered structure (nematic), T_{m2}; and (iii) isotropization, T_{m3}.

During non-isothermal crystallization, the crystallization-peak temperature (T_c) shifted towards a lower temperature with an increase in the cooling rate: the molten samples experienced a shorter time to crystallize fully and hence complete crystallization was not possible with higher rates. In the subsequent heating cycle, two transition processes are clearly visible. With an increase in the cooling rate, the first transition (T_{m1}) shifted slightly towards a higher temperature and the second transition (T_{m2}) shifted toward the lower-temperature region. A further increase in the cooling rate resulted in the two transitions merging into one. These observations can be explained in that with a decreased cooling rate during non-isothermal crystallization, samples get more time to organize crystals and, as a result, there is the possibility of attaining a more-ordered structure. Thus, during heating, the first transition corresponds to a more-ordered to less-ordered transition and the second transition corresponds to isotropization.

The improvement of both moduli of the nanocomposites and, of course, with an increase in the filler concentration in the whole temperature range studied here, is because of the reinforcement effect of the organoclay. Although the nanocomposites also show the same relaxation process as LCP, the first relaxation (first tanδ peak) shifts towards a lower temperature in the nanocomposite samples, compared to the virgin polymer. The second tanδ peak remained unaltered after addition of the clay.

Although under an inert atmosphere, in the case of the nanocomposite samples, initially the degradation started a little earlier, because of the decomposition of the organic modifier present in the organoclay, but after around 8% degradation, the nanocomposite samples show a much higher thermal stability. Here the decomposition occurs by structure-bond rupture or chain scission.

Under an air atmosphere, the nanocomposite samples exhibited higher values of the onset of degradation, along with the two-step decomposition. The first degradation step was mainly due to the chain scission with some extent of oxidation and the second degradation step was due to oxidative reactions. Thus, the first step is mainly a charring process and the second step is a char-combustion process.

Acknowledgements: JB and MB thanks the *Natural Sciences and Engineering Research Council of Canada* (NSERC) for financial support.

Received: June 27, 2007; Revised: August 1, 2007; Accepted: August 3, 2007; DOI: 10.1002/macp.200700350

Keywords: liquid-crystalline polymers; nanocomposites; organoclay; orientation; thermal and thermo-mechanical properties

[1] T.-S. Chung, M. Cheng, P. K. Pallathadka, S. H. Goh, *Polym. Eng. Sci.* **1999**, *39*, 953.
[2] X. Hu, Q. Lin, A. F. Yee, D. Lu, *J. Microsc.* **1997**, *185*, 109.
[3] K. Qi, K. Nakayama, *J. Mater. Sci.* **2001**, *36*, 3207.
[4] [4a] L. Cui, D. R. Paul, *Polymer* **2007**, *48*, 1632; [4b] F. Perrin-Sarazin, M.-T. Ton-That, M. N. Bureau, J. Denault, *Polymer* **2005**, *46*, 11624; [4c] E. Manias, *Mater. Res. Soc. Bull.* **2001**, *26*, 862; [4d] E. Manias, A. Touny, L. Wu, K. Strawhecker, B. Lu, T. C. Chung, *Chem. Mater.* **2001**, *13*, 3516; [4e] A. B. Morgan, J. D. Harris, *Polymer* **2003**, *44*, 2113; [4f] M. Alexandre, P. Dubois, *Mater. Sci. Eng.* **2000**, *R28*, 1.
[5] [5a] N. N. Bhiwankar, R. A. Weiss, *Polymer* **2006**, *47*, 6684; [5b] A. B. Morgan, J. D. Harris, *Polymer* **2004**, *45*, 8695; [5c] J. Zhao, A. B. Morgan, J. D. Harris, *Polymer* **2005**, *45*, 8641.
[6] [6a] K. R. Ratinac, R. G. Gilbert, L. Ye, A. S. Jones, S. P. Ringer, *Polymer* **2006**, *47*, 6337; [6b] N. Salem, D. A. Shipp, *Polymer* **2005**, *45*, 8573.
[7] [7a] N. Ogata, S. Kawakage, T. Ogihara, *J. Appl. Polym. Sci.* **1997**, *66*, 573; [7b] K. E. Strawhecker, E. Manias, *Chem. Mater.* **2000**, *12*, 2943.
[8] [8a] C. I. W. Calcagno, C. M. Mariani, S. R. Teixeira, R. S. Mauler, *Polymer* **2007**, *48*, 966; [8b] G. D. Barber, B. H. Calhoun, R. B. Moore, *Polymer* **2005**, *45*, 6706; [8c] S. S. Lee, Y. T. Ma, H. W. Rhee, J. Kim, *Polymer* **2005**, *45*, 2201.
[9] [9a] S. Sinha Ray, K. Okamoto, M. Okamoto, *Macromolecules* **2003**, *36*, 2355; [9b] S. Sinha Ray, M. Bousmina, *Prog. Mater. Sci.* **2005**, *50*, 962.
[10] S. Sinha Ray, P. Maiti, M. Okamoto, K. Yamada, K. Ueda, *Macromolecules* **2002**, *35*, 3104.
[11] R. A. Vaia, E. P. Giannelis, *Polymer* **2001**, *42*, 1281.
[12] G. Zhang, C. Jiang, C. Su, H. Zhang, *J. Appl. Polym. Sci.* **2003**, *89*, 3155.
[13] W. Huang, C. D. Han, *Macromolecules* **2006**, *39*, 257.
[14] W. Huang, C. D. Han, *Polymer* **2006**, *47*, 4400.
[15] M.-M. Shen, M.-G. Lu, Y.-L. Chen, C.-Y. Ha, *Polym. Int.* **2005**, *54*, 1163.

DOI: 10.1002/macp.200700350

[16] J.-H. Chang, C. H. Ju, S. H. Kim, *J. Polym. Sci., Part B: Polym. Phys.* **2006**, *44*, 387.
[17] Data sheet of Southern Clay Products, Inc. (http://www.nanoclay.com)
[18] D. W. V. Krevelen, "*Properties of Polymers*", Elsevier, Amsterdam 1990.
[19] S. Sinha Ray, M. Okamoto, *Prog. Polym. Sci.* **2003**, *28*, 1539.
[20] R. W. Lenz, *Pure. Appl. Chem.* **1985**, *57*, 977.
[21] H. Fischer, S. Poser, M. Arnold, *Macromolecules* **1995**, *28*, 6957.
[22] S. Sinha Ray, K. Yamada, M. Okamoto, A. Ogami, K. Ueda, *Chem. Mater.* **2003**, *15*, 1456.
[23] [23a] W. Xie, Z. Gao, W. P. Pan, D. Hunter, A. Singh, R. Vaia, *Chem. Mater.* **2001**, *13*, 2979; [23b] J. W. Gilman, W. H. Awad, R. D. Davis, J. Shields, Jr., R. H. Harris, C. Davis, A. B. Morgan, T. E. Sutto, J. Callahan, P. C. Trulove, H. C. DeLong, *Chem. Mater.* **2002**, *14*, 3776; [23c] W. Xie, R. Xie, W. P. Pan, D. Hunter, B. Koene, L. S. Tan, R. Vaia, *Chem. Mater.* **2002**, *14*, 4837.
[24] S. T. Lim, Y. H. Hyun, H. J. Choi, M. S. Jhon, *Chem. Mater.* **2002**, *14*, 1839.